Katsiveli, E., Karamitros, D., Vardanega, P., & Mylonakis, G. (2018). Strain and strain rate effects on the rocking response of footing subjected to machine vibrations. In *Proceedings of the 16th European Conference on Earthquake Engineering* [10760] European Association for Earthquake Engineering (EAEE).

16TH EUROPEAN CONFERENCE ON EARTHQUAKE ENGINEERING THESSALONIKI 18 - 21 JUNE 2018

STRAIN AND STRAIN RATE EFFECTS ON THE ROCKING RESPONSE OF FOOTINGS SUBJECTED TO MACHINE VIBRATIONS

Elpida KATSIVELI[1], Dimitris KARAMITROS [2], Paul J. VARDANEGA[3], George MYLONAKIS[4,5,6]

ABSTRACT

Footings subjected to dynamic loads are commonly designed under the simplifying assumption of linear or equivalent-linear soil behaviour. Even though this approach is simple to implement and, in some cases, could take advantage of available closed-form solutions, the outcomes remain a gross approximation. Although considerable research has been conducted for the case of high-amplitude footing vibrations, where uplift, slippage or even failure may occur, there remains a research gap for small to medium strain amplitudes, for which the behaviour is also non-linear. To address this problem, a numerical methodology is developed herein, for the analysis and design of shallow footings, while taking into consideration shear modulus degradation and hysteretic damping increase effects for the foundation subsoil. The analysis methodology is based on the implementation of the modified hyperbolic model as a user-defined formulation into the explicit finite difference code FLAC. Focus is then given on a rigid strip surface foundation subjected to a harmonic rocking motion, and results from preliminary analyses are presented in terms of the variation of the dynamic impedance with the dimensionless frequency of the excitation. Different excitation amplitudes are examined to demonstrate the effects of soil non-linearity, while strain rate effects are also investigated.

Keywords: shallow foundations; machine vibrations; modified hyperbolic model; strain rate effects

1. INTRODUCTION

The design of machine foundations requires evaluation of the dynamic impedance function (stiffness and damping) of the footing-subsoil system to an externally applied load for one or several degrees of freedom. Apart from the geometrical characteristics of the footing, the impedance function depends on soil material constants and vibration frequency. For elastic analysis, it can be estimated using well-established graphs, charts and regression-based formulae in the literature (e.g., Barkan 1948; Richart et al. 1970; Pais and Kausel 1988; Gazetas 1991; Mylonakis et al. 2006; NIST 2012). However, as the vibration amplitude increases, soil shear modulus decreases in a non-linear fashion and can be modelled as such for fine grained soils of different plasticity (Vucetic and Dobry 1991; Vardanega and Bolton 2013, 2014; Kishida 2017; Wichtmann and Triantafyllidis 2017). Furthermore, in the case of fine-grained soils, shear modulus degradation also becomes sensitive to strain rate effects (e.g., Richardson and Whitman 1963; Matešić and Vucetic 2003; Vucetic and Tabata 2003).

The importance of these non-linearities are explored with the aid of numerical analyses, carried out with the finite difference code FLAC and an implemented non-linear-elastic modified-hyperbolic model (Kondner 1963; Hardin and Drnevich 1972) that accounts for shear modulus degradation and

[1]PhD Student, Department of Civil Engineering, University of Bristol, Bristol, UK, e.katsiveli@bristol.ac.uk
[2]Lecturer, Department of Civil Engineering, University of Bristol, Bristol, UK, d.karamitros@bristol.ac.uk
[3]Lecturer, Department of Civil Engineering, University of Bristol, Bristol, UK, p.j.vardanega@bristol.ac.uk
[4]Professor, Department of Civil Engineering, University of Bristol, Bristol, UK, g.mylonakis@bristol.ac.uk
[5]Professor, Department of Civil Engineering, University of Patras, Patras, Greece
[6]Adjunct Professor, Department of Civil and Environmental Engineering, University of California, Los Angeles, CA, USA

damping increase with both the cyclic shear strain amplitude and the shear strain rate. These simulations allow the extent of non-linearity and its variation with frequency, geometry, material characteristics and loading amplitude to be quantified. For practical design applications, recommendations are made with respect to selection of equivalent-linear parameters, which can be used in combination with existing methodologies, without the need to resort to rigorous numerical investigations. Although this research involves different footing configurations and loading conditions, for the sake of brevity, the focus of this paper is limited to rocking response.

1.1. Problem Description

The configuration examined in this paper is illustrated in Figure 1 as a weightless strip footing of half-width *B*, resting on a clay stratum of thickness *H*, density ρ, shear wave velocity V_s, shear modulus $G = \rho V_s^2$, damping ratio ξ, and Poisson's ratio ν. The footing is subjected to rocking oscillations of amplitude θ, induced by a concentrated harmonic moment *M* as shown in Figure 2 (a). Both the footing and the bedrock underlying the soil layer are assumed to be perfectly rigid, while the soil is modelled as a non-linear material according to the modified hyperbolic model.

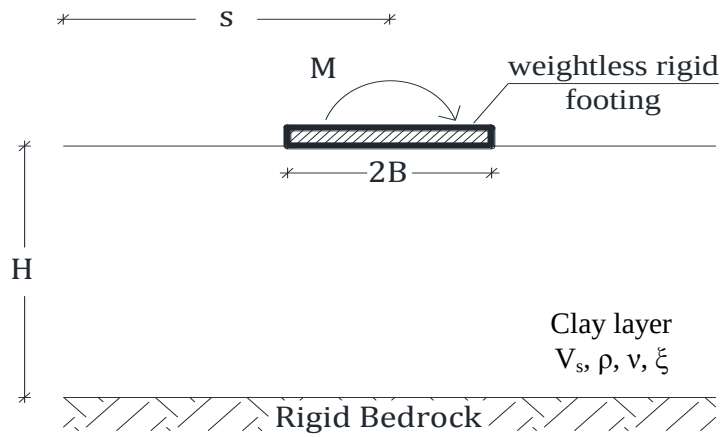

Figure 1. Problem description; footing resting on clay layer

For every response mode, the dynamic soil-foundation system can be analysed using a set of springs and dashpots, the characteristics of which are functions of the input excitation frequency, ω. This frequency dependence originates from the infinite dynamic degrees of freedom of the soil mass (and the associated wave propagation phenomena), which are now condensed to a finite set of degrees of freedom atop the footing. In the case of rocking vibrations, the corresponding dynamic spring of stiffness $\bar{K}_{rx}$ and dashpot with coefficient C_{rx} (Mylonakis et al. 2006) are illustrated in Figure 2(b).

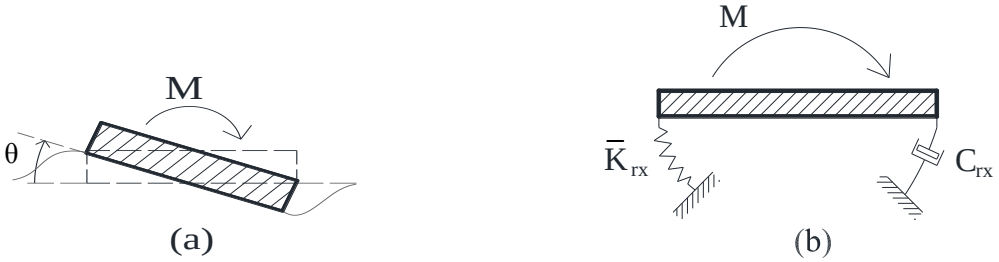

Figure 2. (a) Footing subjected to clockwise moment is rotating towards an angle θ, (b) Spring-dashpot analogue of the footing rocking mode of vibration

When a footing is subjected to a harmonic moment, with amplitude *M* and frequency ω, a harmonic steady-state rotation occurs. In the linear regime, this rotation has the same frequency with the

harmonic moment but is not in phase with the excitation. Using complex notation, the above can be written as:

$$M(\mathrm{t}) = M \exp(i\omega t) \tag{1}$$

and

$$\theta(t) = \theta \, exp(i\omega t) \tag{2}$$

where M and θ are generally not in phase, so θ in Equation (2) is typically complex valued. Therefore, the dynamic impedance can be expressed in the form of Equation (3):

$$K_{rx} = \frac{M(\mathrm{t})}{\theta(\mathrm{t})} = \bar{K}_{rx} + i \, \omega \, C_{rx} \tag{3}$$

in which the complex exponents in Equations (1) and (2) cancel out from the numerator and the denominator. Note that this cancellation is not possible with ordinary trigonometric functions, which highlights the usefulness of using complex notation in such problems. Although the above expressions apply to all modes of excitation (translational and rotational), this paper focuses solely on the rocking mode.

For static conditions and under the assumption of a smooth soil-footing interface, Muskhelishvili (1963) (cited in Poulos and Davis 1974 p. 165) derived an exact solution for the rocking stiffness, which can be expressed in the form shown as Equation 4.

$$K_{rx,elastic} = \frac{\pi}{2\,(1-\nu)} GB^2 \tag{4}$$

Note that rocking stiffness is measured in units of force in accordance with the plane-strain nature of the problem. In the presence of rock at a shallow depth Gazetas (1983) introduced an empirical correction factor to the above solution, to account for the soil layer thickness.

$$K_{rx,elastic} \simeq \frac{\pi}{2\,(1-\nu)} \, GB^2 \left(1 + 0.2\frac{B}{H}\right) \tag{5}$$

where H is the thickness of the soil layer. For dynamic conditions, the dynamic stiffness $\bar{K}_{\mathrm{rx}}$ is obtained by multiplying the above static values with the following approximate dynamic stiffness modification coefficient introduced by Gazetas (1983) based on the results by Luco and Westmann (1972):

$$k_{rx} \simeq 1 - 0.2 \, \alpha_0 \tag{6}$$

where $\alpha_0 = 2\pi f \, B/V_s$ is the familiar dimensionless frequency. In light of this expression, the dynamic stiffness at α_0 = 5 is zero and beyond that becomes negative. This should not come as a surprise, as a zero value for $\bar{K}_{\mathrm{rx}}$ merely suggests that inertia forces perfectly balance the elastic ones in the soil medium, while negative stiffness (which is inadmissible for static conditions) implies a phase difference between excitation and response greater than 90^{o}.

2. NUMERICAL ANALYSIS METHODOLOGY

2.1 FLAC 7.0 Finite Difference Code

All the analyses were carried out using FLAC 2D version 7.0, commercial software developed by Itasca Inc (2011). FLAC (an abbreviation for Fast Lagrangian Analysis of Continua) is a two-dimensional explicit finite difference code for geotechnical engineering applications, which allows the

implementation of user-defined constitutive models (UDMs), written in C++ and compiled as Dynamic Link Libraries (DLL files). Due to the explicit nature of the integration algorithm, the main UDM function is to return new stresses given the current stress condition and the applied strain increment, namely a procedure that is rather straightforward even for complicated constitutive laws. This functionality is utilized herein, for the implementation of the modified hyperbolic model, as outlined in the following section.

Furthermore, FLAC contains a built-in programming language, FISH, which enables the user to define new variables and functions. These functions are compiled and stored in FLAC's memory space and hence they can be executed parallel to the analysis. In this case, FISH is used to prescribe a variation of model properties across the grid (mesh), as a function of the strain-rate given by FLAC for every zone (element) during every time-step. This allows the accurate implementation of strain-rate effects, as presented in Section 4.

2.2 Modified Hyperbolic Model

The modified hyperbolic model (used in Darendeli 2001; Zhang et al. 2005; Vardanega and Bolton 2013, 2014) is based on the hyperbolic model, with the addition of a curvature parameter. The secant shear modulus reduction curve (MR curve) for this model is described as:

$$\frac{G_s}{G_{max}} = \frac{1}{1+\left(\frac{\gamma}{\gamma_r}\right)^a} \tag{7}$$

where γ_r is a pseudo-reference shear strain which is equal to the level of shear strain for which G_s/G_{max}= 0.5, while α is a curvature coefficient as illustrated in Figure 3. The parameters α and γ_r are predominantly determined through experiments conducted on the soil type of interest. The model has been found reliable to maximum shear strains of about 0.1 to 0.3% and should not be used in the vicinity of the soil shear strength.

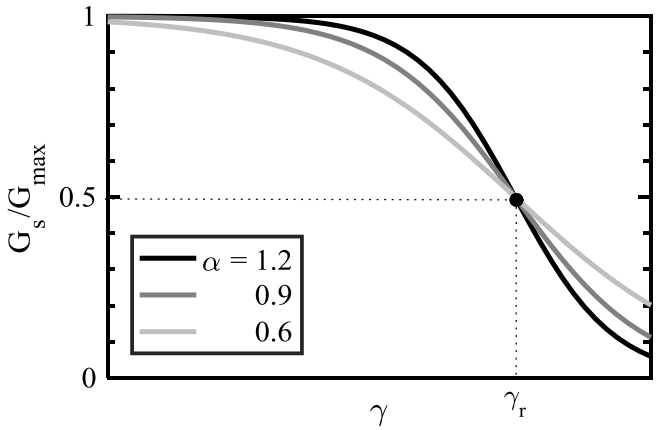

Figure 3. Illustration of reference strain and the effect of curvature parameter on the shape of the modulus reduction curve

2.3 Model Implementation

Implementation of the modified hyperbolic model into an incremental solution algorithm such as FLAC, requires the tangent shear modulus G_t to be derived from Equation (7) and given here as Equation (8):

$$\frac{G_t}{G_{max}} = \frac{1}{G_{max}} \frac{d(G_s \gamma)}{d\gamma} = \frac{1+(1-\alpha)\left(\frac{\gamma}{\gamma_r}\right)^{\alpha}}{\left[1+\left(\frac{\gamma}{\gamma_r}\right)^{\alpha}\right]^2} \tag{8}$$

As described in the above, user-defined models in FLAC must calculate stress increments as a function of the current stress state and the applied strain increment. As a result, Equation 8, where G_t is expressed in terms of the total developing strain γ, cannot be directly applied. To obtain G_t as a function of the current shear stress τ, Equation 7 is substituted in $\tau = G_s \gamma$:

$$\frac{\tau}{G_{max}}\left[\left(\frac{\gamma}{\gamma_r}\right)^{\alpha} + 1\right] - \gamma = 0 \tag{9}$$

The tangent shear modulus G_t can be obtained by solving Equation 9 for γ and substituting the result back into Equation 8.

In the case of $\alpha = 1$ or $\tau = 0$, solving Equation 9 is trivial. However, for $\alpha \neq 1$ and $\tau \neq 0$, no general analytical solution is available. Therefore, the Newton-Raphson procedure is incorporated in the implementation algorithm and γ is computed iteratively, as:

$$\gamma_n = \gamma_{n-1} - \frac{\frac{\tau}{G_{max}}\left[\left(\frac{\gamma_{n-1}}{\gamma_r}\right)^{\alpha}+1\right]-\gamma_{n-1}}{\frac{\tau}{G_{max}}\frac{\alpha}{\gamma_{n-1}}\left(\frac{\gamma_{n-1}}{\gamma_r}\right)^{\alpha-1}-1} \tag{10}$$

Nevertheless, the function in Equation 9 is not monotonic, as its derivative (hence also the denominator in Equation 10) becomes zero for a critical value of γ, namely:

$$\gamma_{cr} = \left(\frac{G_{max}\,\gamma_r^{\alpha}}{\alpha\,\tau}\right)^{\frac{1}{\alpha-1}} \tag{11}$$

Therefore, to ensure convergence to the correct root γ, an appropriate value of γ_1 needs to be selected for the first iteration. For $\alpha < 1$, there exists only one positive solution which is always obtained if the initial value is $\gamma_1 > \gamma_{cr}$ (e.g., $\gamma_1 = 10\,\gamma_{cr}$).

In the case of $\alpha > 1$, the modified hyperbolic model predicts a peak shear stress. The shear strain at which this is occurring can be obtained by setting $G_t = 0$ in Equation 8:

$$\gamma_{peak} = \left(\frac{1}{1-\alpha}\right)^{\frac{1}{\alpha}} \gamma_r \tag{12}$$

The peak stress can be then calculated by replacing Equation 12 into Equation 9:

$$\tau_{\text{peak}} = G_{max}(\alpha-1)^{1-\frac{1}{\alpha}}\frac{\gamma_r}{\alpha} \tag{13}$$

For $\gamma > \gamma_{peak}$, the tangent shear modulus becomes negative, while, using Equation 7, it can be easily shown that for $\gamma \to \infty$, $\tau \to 0$. As a result, for $\alpha > 1$ and $\tau < \tau_{peak}$, Equation 10 has two positive roots. To ensure convergence to the appropriate one, the following procedure is followed: In the beginning of each loading cycle, the initial value for the Newton Raphson iterations is selected as $\gamma_1 < \gamma_{cr}$ (e.g., $\gamma_1 = 0$). Once the peak shear stress is reached, the initial value for each iteration is selected as $\gamma_1 > \gamma_{cr}$ (e.g., $\gamma_1 = 2\gamma_{cr}$). This algorithm has been tested extensively and has been found to always converge with an accuracy of $\gamma \pm 10^{-8}$ within a maximum of 5-10 iterations.

Following the above, the model is implemented into FLAC using the following non-linear elastic formulation (expressed using Kronecker's δ symbol):

$$\dot{\sigma}_{ij} = G_t(\sigma_{ij}) \cdot \left(\delta_{ik}\delta_{kl} + \delta_{il}\delta_{jk} + \frac{2\nu}{1-2\nu}\delta_{ij}\delta_{kl}\right) \cdot \dot{\varepsilon}_{kl} \quad (14)$$

where ν is Poisson's ratio, which is assumed to remain constant. To obtain the tangent shear modulus as a function of the current multiaxial stress state, the shear stress τ in Equation 10 is replaced by:

$$X_\tau = \sqrt{\frac{1}{2}(s_{ij} - s_{ij}^{LR})(s_{ij} - s_{ij}^{LR})} \quad (15)$$

where s_{ij} is the deviatoric stress $s_{ij} = \sigma_{ij} - \delta_{ij}\sigma_{kk}/3$, while s_{ij}^{LR} is the deviatoric stress at the beginning of the analysis or at the last shear reversal. Finally, to allow for the formation of closed τ-γ loops, after the first shear reversal, the reference shear strain γ_r is replaced by $\gamma_r' = 2\gamma_r$.

2.4 Finite Difference Grid

The finite difference grid utilized in the analyses is shown in Figure 4.

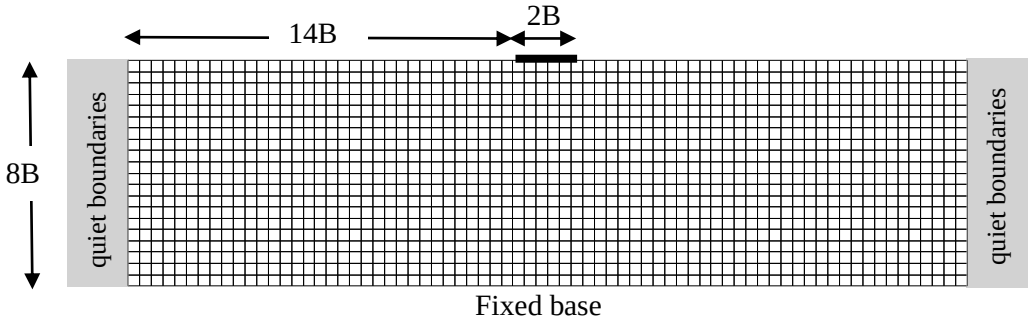

Figure 4. View of typical finite difference 2-D mesh

More specifically, a grid of width (14 *B*) was used, with a total depth of (8 *B*), where *B* is the half-width of the footing. In this case, a value of *B* = 2.5m was selected, although the results can be readily generalized to other footing widths. Quiet boundaries were employed at the sides of the model, while movements at the base were fixed in both directions. The model was discretized to square elements of (0.4 *B*). Note that the accuracy of this discretization was verified through rigorous mesh sensitivity analyses.

Soil behaviour was simulated using the aforementioned Modified Hyperbolic Model. A shear wave velocity of V_s = 158m/s and a soil mass density ρ = 2Mg/m^3 were considered, resulting in a maximum shear modulus G_{max} = 50MPa. The Poisson's ratio was taken as ν = 0.35. In the dynamic analyses, a Rayleigh damping was also incorporated, namely ξ = 3% to account for soil damping at small shear strain amplitudes. For larger amplitudes, additional hysteretic damping was obtained inherently from the non-linear response of the implemented soil model. It should be noted that damping has a minor influence in the stiffness values reported in this work and won't be discussed further.

Finally, the footing rotation was applied as a prescribed velocity or acceleration imposed to the corresponding model nodes. The reactions at these nodes allowed to calculate, using FLAC's inbuilt programming language FISH, the corresponding developing moment. Since the implemented model does not account for failure, the initial loading applied to the model does not affect the obtained results. Nevertheless, the obtained response is only valid for medium factor-of-safety values (e.g., *FS* = 2 to 3) and small-to-medium moments/rotations, when the applied cyclic loading does not induce bearing capacity failure or foundation uplifting.

3. VERIFICATION

3.1 Footing resting on linear elastic soil subjected to static loading

Firstly, a linear static analysis was carried out to evaluate FLAC's performance in rocking response. The scope of this analysis is to prove the suitability of model dimensions and boundary fixities on the accuracy of stiffness calculation. For the case examined herein, Equation 5 predicts a rocking stiffness $K_{rx,elastic}$ = 7.74 x 10^5 kN/m^2. This is in notably good agreement (less than 0.7% discrepancy) with the numerically obtained value of 7.79 x 10^5 kN/m^2.

3.2 Footing resting on linear elastic soil subjected to dynamic loading

Following static loading, linear dynamic analyses were conducted for non-dimensional frequency values ranging between 0 and 1.2. The sinusoidal input motion used for the dynamic analyses is shown in Figure 5, in terms of the acceleration applied directly on the footing. Only the constant amplitude part of the sinusoidal motion (20 cycles) is accounted for in the stiffness and damping coefficient calculations.

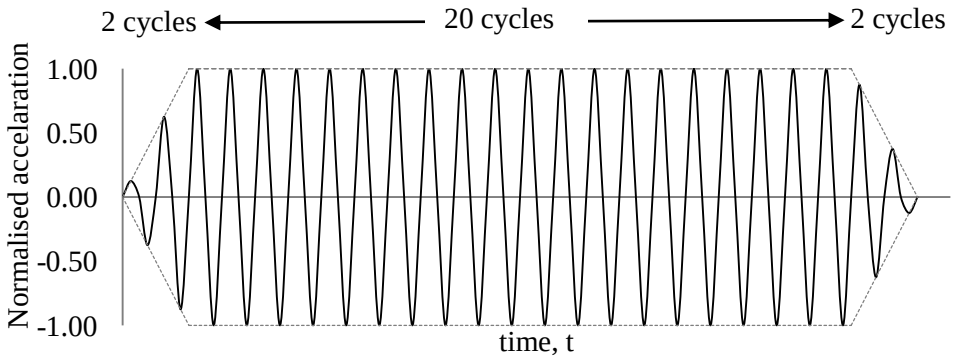

Figure 5. Sinusoidal input motion expressed in terms of acceleration applied directly on the rigid footing

Results from the numerical analyses are compared against the classical semi-analytical solution by Luco and Westmann (1972) and they are shown below in Figure 6. A very good agreement is observed for dimensionless frequencies a_0 of less than approximately 0.6. The discrepancies observed at higher frequencies might be attributed to differences in the boundary conditions between the two solutions.

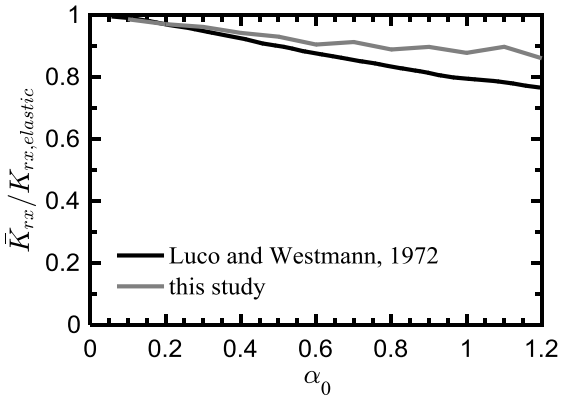

Figure 6. Evaluation of linear dynamic analyses

4. PARAMETRIC INVESTIGATION

4.1. Non-linear analyses

In order to accurately capture non-linear soil-structure interaction effects, it is essential to simulate non-linear soil behaviour at small and medium cyclic shear strain amplitudes. In this case, the response is governed by a hysteretic behaviour, which can be modelled using non-linear elastic stress-strain relationships. Soil shear modulus reduces with increasing strain and this reduction can be approximated by various forms of a hyperbolic function (e.g., Kondner, 1963; Hardin and Drnevich 1972; Darendeli 2001; Zhang et al. 2005). Specific studies for databases of sands have been published (e.g., Oztoprak and Bolton 2013; Wichtmann and Triantafyllidis 2013a, 2013b) and for fine grained soils (e.g., Vardanega and Bolton 2013, 2014; Wichtmann and Triantafyllidis 2017). For the analysis presented in this paper soil non-linearity was explored by means of a modified hyperbolic model (equation 7).

4.1.1 Database analysis

Vardanega and Bolton (2013) corrected a database of 67 tests on 21 fine grained soils for the influence of rate effects assuming a 5% reduction per log cycle (an assumption made based on the findings of Lo Presti et al. 1997 and d'Onofrio et al. 1999). The analysis of the database produced expressions for the reference stain linked to plasticity index (following the observations of Vucetic and Dobry 1991). For the *static adjustment*, the curvature parameter and the reference strain were shown to be linked to changes in plasticity via the empirical relationships shown as equation 16:

$$\alpha = 0.736\,,\ \ \gamma_r = 2.2\left(\frac{I_p}{1000}\right) \tag{16}$$

while for the *dynamic adjustment* the curvature parameter and the reference strain were shown to be linked to changes in plasticity via the empirical relationships shown as equation 17:

$$\alpha = 0.943,\ \ \gamma_r = 3.7\left(\frac{I_p}{1000}\right) \tag{17}$$

which correspond to a strain rate of 10^{-2}/s. Note that I_p is expressed numerically for both equations (16) and (17).

4.1.2 Parametric range investigated

The modified hyperbolic model parameters α, γ_r alter depending on the strain rate correction applied. In the initial set analysis for this paper the α and γ_r was held constant and were taken to be $\alpha = 0.736$ and $\gamma_r = 1.1 \cdot 10^{-3}$ (using Equations 16), which describes a *static adjustment (STA)*. A second set of analyses is conducted with the parameter values $\alpha = 0.943$ and $\gamma_r = 1.85 \cdot 10^{-3}$ (using Equations 17), which describes a *pseudo shear strain rate adjustment (PSSR)* in the model. Using these sets of parameters, analyses were carried out for both static and dynamic rocking loads.

Nevertheless, a rigorous analysis of the problem also requires considering the variation of shear strain rates across the foundation subsoil. To achieve this, a third set of analyses was carried out, more accurately accounting for shear strain rate effects, by appropriately varying the model parameters with location and with time, a function of the shear strain rate in each element of the mesh. As a first approximation, the expressions used for intermediate values of strain rates were obtained from linear interpolation between the two aforementioned sets of limiting values (STA and PSSR) see Figure 7.

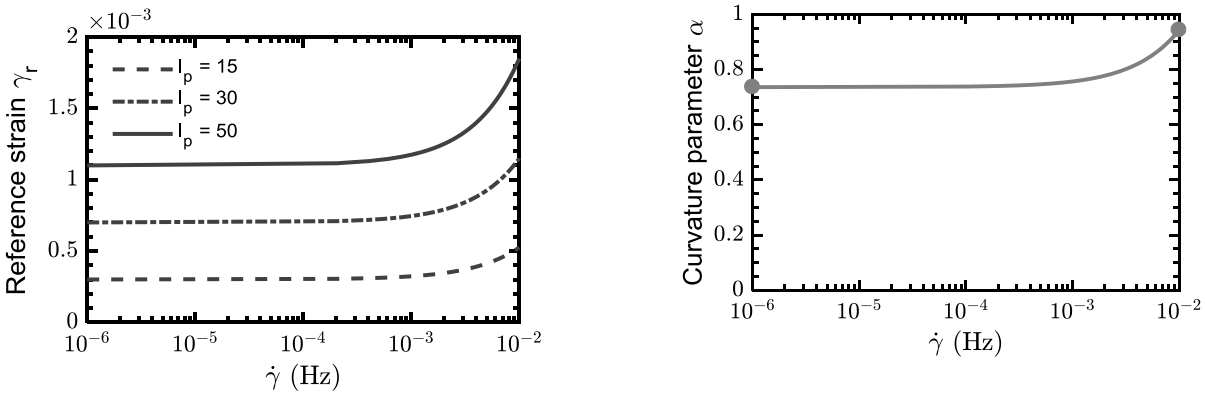

Figure 7. Modified hyperbolic model parameter γ_r (left) and α (right) as functions of the strain rate (units of frequency).

5. RESULTS

The results are illustrated in Figure 8. In vertical axes, static values of normalised nonlinear rocking stiffness $K_{rx}/K_{rx,elastic}$ are plotted versus the rocking angle θ (left graph) and θ normalised by the reference strain γ_r (right graph). Evidently, stiffness degradation might be stronger for the case of pseudo-shear strain rate parameters, notably beyond $\theta = 10^{-4}$ and $\theta/\gamma_r = 10^{-1}$. In these curves, the effect of model parameters is also evident. Overall, the increase in stiffness due to pseudo strain rate effects does not exceed 10% or so.

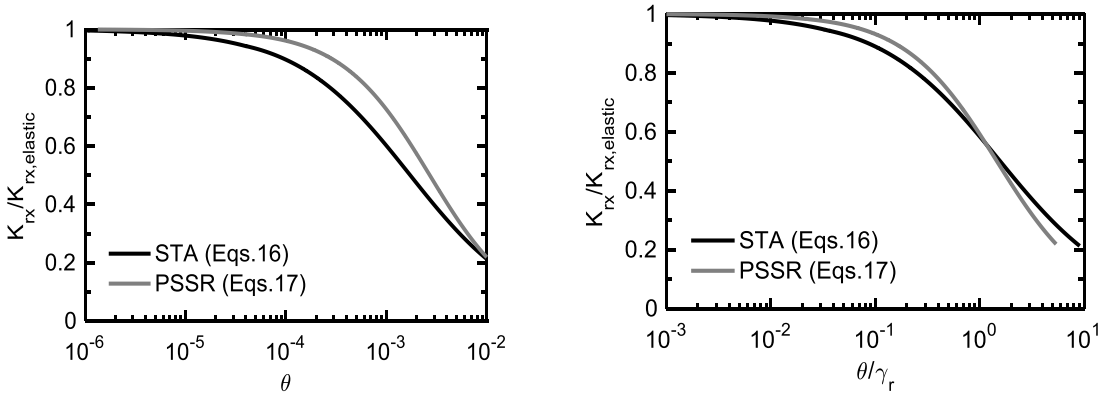

Figure 8. Normalised static rocking stiffness versus rocking angle (left) and normalised rocking angle (right)

The curves in Figure 8 can be fitted by a modified hyperbolic expression of normalised nonlinear rocking stiffness as a function of rocking angle normalised by a 'pseudo-reference' rocking angle, θ_r

$$\frac{K_{rx}}{K_{rx,elastic}} = \frac{1}{1+\left(\frac{\theta}{\theta_r}\right)^a} \tag{18}$$

where θ_r is the 'pseudo-reference' rocking angle equals to $1.5 \cdot \gamma_r$, and γ_r, α as specified in equations (16) and (17) for static and dynamic adjustment, respectively.

Results for dynamic conditions are reported in Figure 9, where the nonlinear dynamic rocking stiffness is plotted in normalised form as $\overline{K}_{rx}/K_{rx,\ elastic}$ (left graph) and $\overline{K}_{rx}/K_{rx}$ (right graph) versus the dimensionless excitation frequency $a_0 = 2\pi f\ B/V_s$ for three different rocking amplitudes θ_{max} (10^{-5}, 10^{-4}, 10^{-3}).

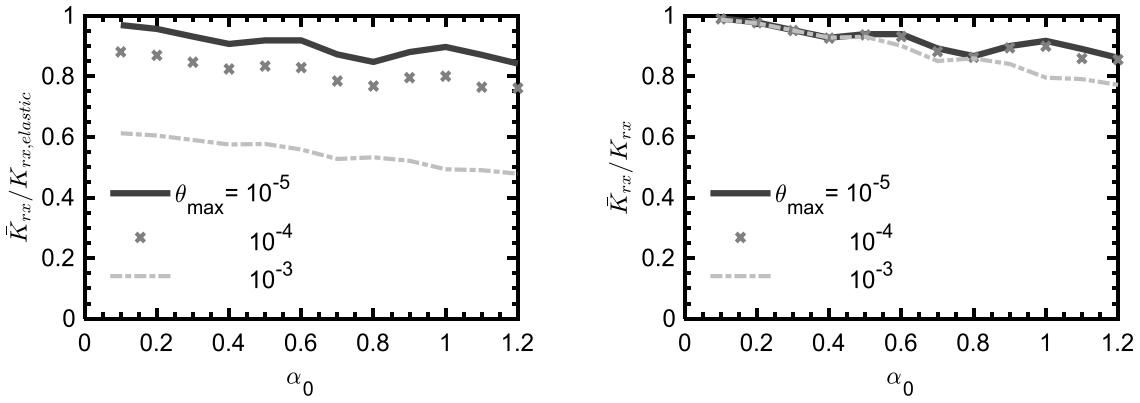

Figure 9. Normalised nonlinear dynamic rocking stiffness over elastic (left) and non-linear (right) static rocking stiffness versus dimensionless frequency for different rotation amplitudes. Modified hyperbolic model parameters correspond to STA conditions according to Equation (16).

No rate effects have been considered in this plot (STA conditions). Despite the different levels of soil nonlinearity involved in the analysis, the frequency variation in the three curves follows that of the elastic model in Figure 5. This is particularly evident in the right graph and suggests that the nonlinearity mainly affects the static stiffness K_{rx}, while the dynamic stiffness modifier k_{rx} can still be obtained from the elastodynamic Equation (6) for dimensionless frequencies a_o as high as 0.8.

Analogous patterns are observed in Figure 10 where the normalised nonlinear dynamic rocking stiffness is plotted versus dimensionless frequency using the pseudo shear strain rate (PSSR) adjustment according to Equations 17. The behaviour is like the previous case, with all curves exhibiting similar frequency variations, independent of strain level, and nonlinearity affecting primarily the static stiffness term K_{rx}.

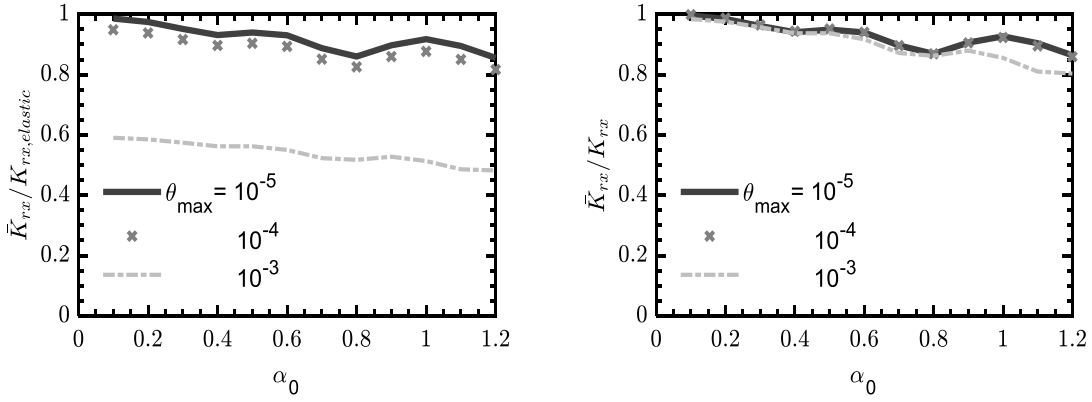

Figure 10. Normalised nonlinear dynamic rocking stiffness over elastic (left) and non-linear (right) static rocking stiffness versus dimensionless frequency for different rotation amplitudes. Modified hyperbolic model parameters correspond to PSSR conditions according to Equation (17)

Results for shear strain rate (SSR) effects on nonlinear dynamic footing stiffness $\bar{K}_{rx}$ are provided in Figure 11. Since the model is formulated in terms of absolute strain rate (measured in units of 1/Time, Figure 6), use of dimensionless frequency a_0 is not possible. For the small rocking amplitudes $\theta_{max} = 10^{-5}$ and 10^{-4}, the curves exhibit patterns analogous to those observed for STA and PSSR conditions in Figures 9 and 10. For the largest rocking amplitude ($\theta_{max} = 10^{-3}$), however, a different pattern is observed, with the nonlinear rocking stiffness increasing with frequency. The causes of this behaviour could be sought to stress-induced inhomogeneities in the soil mass, as strain rate varies for

point to point in proportion to strain. Further research is required to quantify this effect.

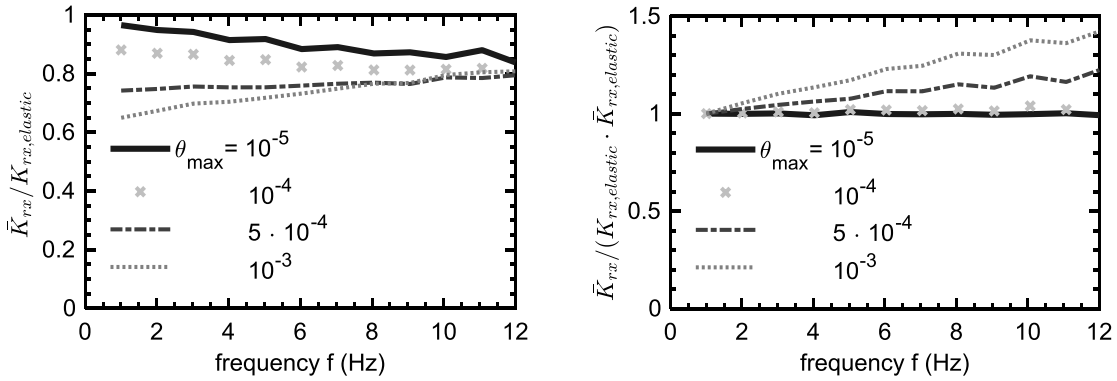

Figure 11. Normalised nonlinear dynamic rocking stiffness over elastic static rocking stiffness (left) and additionally over the elastic dynamic rocking stiffness as shown in Figure 6 (right) versus absolute frequency for different rotation amplitudes. Modified hyperbolic model parameters correspond to SSR conditions according to Figure 7.

6. CONCLUSIONS

The main conclusions of the study are summarized in the following:

- A practical numerical methodology for nonlinear analysis of rigid surface footings under rocking oscillations, was presented. A modified hyperbolic model originally calibrated using an experimental database was implemented into the finite difference code FLAC, to account for stress-strain and shear strain rate behaviour of soil. The two required model parameters, α and γ_r, can either be constant, pertaining to static or dynamic conditions, or vary as a function of shear strain rate.
- Parametric analyses on shear rate effects showed that for rocking amplitudes θ_{max} = 10^{-5} and 10^{-4} nonlinear dynamic rocking stiffness is fluctuating past α_0= 0.4 following a very similar trend to the linear case. For the rocking amplitude of 10^{-3} the values are dropping significantly, and curves are smoother. This suggests that nonlinearity mainly affects the static stiffness K_{rx}, while the dynamic stiffness modifier k_{rx} can be obtained from the elastodynamic Equation (6) for dimensionless frequencies α_0 as high as 0.8. The drop in static stiffness can be explained by shear modulus degradation effects, as shown in Figure 7.
- Regarding SSR effects, an increase in rocking stiffness is observed with increasing frequency for the largest rocking amplitude (θ_{max} = 10^{-3}). The causes of this behaviour may be related to stress-induced inhomogeneity in the soil mass, as shear strain rate varies for point to point in proportion to strain. On the other hand, for small rotation amplitudes stiffness is unaffected by shear strain rate which shows that, in this case, soil non-linearity would be of minor importance.
- SSR effects are becoming evident from very low frequencies for rocking amplitudes larger than θ_{max} = 10^{-4} and they are increasingly more significant with increasing frequency. For rocking amplitudes equal or under θ_{max} = 10^{-4}, non-linearity and SSR effects have negligible impact on dynamic stiffness.
- Finally, the results presented in this paper should be verified experimentally. Carefully designed model tests in controlled environments (e.g., in geotechnical centrifuges, shaking tables and soil pits) would be useful in this regard.

7. ACKNOWLEDGMENTS

The first author acknowledges the financial support which has been provided through the Engineering and Physical Sciences Research Council (EPRSC) Doctoral Training Partnership (DTP) studentship.

8. REFERENCES

Barkan DD (1948). Dynamics of Beds and Foundations [in Russian], Stroivoenmorizdat, Moscow.

Darendeli MB (2001). Development of a new family of normalized modulus reduction and material damping curves. *Ph.D. thesis*, University of Texas at Austin, Austin, TX, United States of America.

d'Onofrio A, Silvestri F, Vinale F (1999). Strain rate dependent behaviour of a natural stiff clay. *Soils and Foundations*, 39(2): 69-82.

Gazetas G (1983). Analysis of Machine Foundation Vibrations: State of the Art. *International Journal of Soil Dynamics and Earthquake Engineering*, 2(1): 2-42.

Gazetas G (1991). Foundation Vibrations. In: Foundation Engineering Handbook 2nd Ed. (Fan, H-S. ed.), Boston, MA: Springer US.

Hardin BO, Drnevich VP (1972). Shear Modulus and Damping in Soils: Design Equations and Curves. *Journal of the Soil Mechanics and Foundations Division (American Society of Civil Engineers)*, 98(7): 667-692.

Itasca Inc. (2011). FLAC: Fast Lagrangian Analysis of Continua (Version 7). Minneapolis, Minnesota, United States of America.

Kishida T (2017). Comparison and Correction of Modulus Reduction Models for Clays and Silts. *Journal of Geotechnical and Geoenvironmental Engineering (American Society of Civil Engineers)*, 143(4): 04016110.

Kondner RL (1963). Hyperbolic Stress-Strain Response: Cohesive Soils. *Journal of the Soil Mechanics and Foundation Division (American Society of Civil Engineers)*, 89(1): 115-144.

Lo Presti DCF, Jamiolkowski M, Pallara O, Cavallaro A, Pedroni S (1997). Shear modulus and damping of soils. *Géotechnique*, 47(3): 603–617.

Luco JE, Westmann RA (1972). Dynamic response of a rigid footing bonded to an elastic half space. *Journal of Applied Mechanics*, 39(2): 527-534.

Matešić L, Vucetic M (2003). Strain-Rate Effect on Soil Secant Shear Modulus at Small Cyclic Strains. *Journal of Geotechnical and Geoenvironmental Engineering (American Society of Civil Engineers)*, 129(6): 536-549.

Muskhelishvili NI (1963). Some basic problems of the mathematical theory of elasticity. Noordhoff, Gronigen.

Mylonakis G, Nikolaou S, Gazetas G (2006). Footings under Seismic Loading: Analysis and Design Issues with Emphasis on Bridge Foundations. *Soil Dynamics and Earthquake Engineering*, 26(9): 824-853.

National Institute for Standards and Technology (NIST) (2012). Soil-Structure Interaction for Building Structues. *NIST GCR 12-917-21*, National Institute for Standards and Technology, US Department of Commerce. http://www.nehrp.gov/pdf/nistgcr12-917-21.pdf (accessed 04/03/2018).

Oztoprak S, Bolton MD (2013). Stiffness of sands through a laboratory test database. *Géotechnique*, 63(1): 54–70.

Pais A, Kausel E (1988). Approximate formulas for dynamic stiffnesses of rigid foundations. *Soil Dynamics and Earthquake Engineering*, 7(4): 213-227.

Poulos HG, Davis EH (1974). Elastic solutions for soil and rock mechanics. John Wiley & Sons, New York, NY, United States of America.

Richardson AM, Whitman RV (1963). Effect of strain-rate upon undrained shear resistance of a saturated remoulded fat clay. *Géotechnique*, 13(4): 310-324.

Richart FE, Hall JR, Woods, RD (1970). Vibrations of Soils and Foundations. Prentice Hall, Englewood Cliffs, NJ, United States of America.

Vardanega, PJ, Bolton MD (2013). Stiffness of Clays and Silts: Normalizing Shear Modulus and Shear Strain. *Journal of Geotechnical and Geoenvironmental Engineering (American Society of Civil Engineers)*, 139(9): 1575-1589.

Vardanega PJ, Bolton MD (2014). Stiffness of Clays and Silts: Modeling Considerations. *Journal of Geotechnical and Geoenvironmental Engineering (American Society of Civil Engineers)*, 140(6): 06014004.

Vucetic M, Dobry R (1991). Effect of Soil Plasticity on Cyclic Response. *Journal of Geotechnical and Engineering (American Society of Civil Engineers)*, 117(1): 89-107.

Vucetic M, Tabata K (2003). Influence of Soil Type on the Effect of Strain Rate on Small Strain Cyclic Shear Modulus. *Soils and Foundations*, 43(5): 161-173.

Wichtmann T, Triantafyllidis T (2013a). Effect of uniformity coefficient on G/G_{max} and damping ratio of uniform to well-graded quartz sands. *Journal of Geotechnical and Geoenvironmental Engineering (American Society of Civil Engineers)*, 139(1): 59-72.

Wichtmann T, Triantafyllidis T (2013b). Stiffness and damping of clean quartz sand with various grain-size distribution curves. *Journal of Geotechnical and Geoenvironmental Engineering (American Society of Civil Engineers)*, 140(3): 06013003.

Wichtmann T, Triantafyllidis T (2017). Monotonic and cyclic tests on kaolin: a database for the development, calibration and verification of constitutive models for cohesive soils with focus to cyclic loading. *Acta Geotechnica*, http://dx.doi.org/10.1007/s11440-017-0588-3.

Zhang J, Andrus RD, Juang CH (2005). Normalized shear modulus and material damping ratio relationships. *Journal of Geotechnical and Geoenvironmental Engineering (American Society of Civil Engineers)*, 131(4): 453–464.